Forward modelling of oceanic lithospheric magnetization

S. M. Masterton,[1,*] D. Gubbins,[1,2] R. D. Müller[2] and K. H. Singh[3]

[1]*School of Earth & Environment, University of Leeds, Leeds LS2 9JT, UK. E-mail: sheona.masterton@getech.com*
[2]*School of Geosciences, University of Sydney, NSW, Australia*
[3]*Department of Earth Sciences, Indian Institute of Technology, Mumbai, India*

SUMMARY
We construct a model of remanence for the oceans, combine it with a model of induced magnetization for the whole Earth from a previous study, compute the predicted lithospheric geomagnetic field and compare the result with a model, MF7, that is based on satellite data. Remanence is computed by assigning magnetizations to the oceanic lithosphere acquired at the location and time of formation. The magnetizing field is assumed to be an axial dipole that switches polarity with the reversal time scale. The magnetization evolves with time by decay of thermal remanence and acquisition of chemical remanence. The direction of remanence is calculated by Euler rotation of the original geomagnetic field direction with respect to an absolute reference frame, significantly improving previous results which did not include realistic oceanic magnetization computed this way. Remanence only accounts for 24 per cent of the energy of the oceanic magnetization, the induced magnetization being dominant, increasing slightly to 30 per cent of the part of the magnetization responsible for generating geomagnetic anomalies and 39 per cent of the Lowes energy of the geomagnetic anomalies. This is because our model of oceanic crust and lithosphere is fairly uniform, and a uniform layer magnetized by a magnetic field of internal origin produces no external field. The largest anomalies are produced by oceanic lithosphere magnetized during the Cretaceous Normal Superchron. Away from ridges and magnetic quiet zones the prediction fails to match the MF7 values; these are also generally, but not always, somewhat smaller than the observations. This may indicate that the magnetization estimates are too small, in which case the most likely error is in the poorly-known magnetization deep in the crust or upper mantle, or it may indicate some other source such as locally underplated continental lithosphere or anomalous oceanic crust, or even small-scale core fields.

Key words: Magnetic anomalies: modelling and interpretation; Rock and mineral magnetism; Satellite magnetics; Mid-ocean ridge processes.

1 INTRODUCTION

The *Decade of Geopotential Research* has provided geomagnetic data from satellites with unprecedented accuracy and coverage (Friis-Christensen *et al.* 2009), while the next mission, a constellation of satellites called *Swarm* (Friis-Christensen & Luhr 2006; Olsen & Kotsiaros 2011) (expected launch Spring 2013), will continue the mapping exercise to even finer resolution and accuracy. Models of the geomagnetic field now extend to very fine spatial resolution (Maus *et al.* 2009); they contain some clear signals from known structures in the oceanic lithosphere (Maus *et al.* 2008) and a great many unexplained features also arising from magnetized rocks in the crust and upper mantle. The new, fine resolution, geomagnetic

data offer fresh insight into the identification and understanding of buried structures in the crust and lithosphere.

The ideal approach would be to invert magnetic field data for magnetization structures in the crust and lithosphere, but unfortunately, this is far from straightforward. Like all potential field methods, magnetics suffers from a fundamental ambiguity: many distributions of magnetization produce no observable magnetic field whatsoever and therefore remain 'invisible'. In a companion paper (Gubbins *et al.* 2011), we separate the 'visible' and 'invisible' parts of a realistic global model of vertically integrated magnetization (VIM) and show it to be dominated by the invisible part, which is almost 90 per cent of the magnetization. Inversion of geomagnetic field data for magnetization is unwise in the presence of such a large null space: constraints that do not involve additional data in some form, such as simple mathematical definitions of what constitutes the 'simplest' structure, would lead to highly misleading maps of

*∗ Present address: GETECH, Leeds, UK.

magnetization. To be successful, any constraint must be strong and based on additional data, from seismology, mineralogy, or geological maps for example. Assuming that the magnetization is purely induced in a known inducing field reduces the problem from one of determining a vector magnetization to one of determining a scalar susceptibility, but this involves further ambiguities, as Maus & Haak (2003) have shown.

A forward-problem approach, in which magnetic fields are calculated from candidate structures, the results compared with observation, then revised to improve the fit, is our favoured method for interpreting the new lithospheric field models. Forward modelling has been used by several authors in both regional and global studies.

Hemant & Maus (2005) adopted a geographic information system (GIS) approach to forward-model global magnetic anomalies at satellite altitude. They assumed that all magnetization on continents is induced. In nine Precambrian cratons, they assigned susceptibilities in each of three layers, the values being appropriate to the rock type to where stratigraphy is available. In all other geological provinces, they used two layers, the upper layer having a blanket susceptibility typical of sediments, the lower layer one appropriate for the basement age where known. The susceptibility of lower crust was assumed to be 1.2 or 1.6 times that of the upper crust for Archean or post-Archean provinces, respectively. These values were based on ferrous oxide ratios for upper/lower crust (Taylor & McLennan 1985). Lower crustal thickness was also given by seismic models, consistent with the assumption that the base of the magnetized crust coincides with the Moho seismic discontinuity (Wasilewski & Mayhew 1992). Crustal thickness was given by global seismic models 3SMAC (Nataf & Ricard 1996) and CRUST2.0 (Bassin *et al.* 2000). Induced magnetization in the oceans was represented by three layers of uniform thickness down to the Moho. Continental and island arcs were modelled as two-layer structures, the upper layer being granite and granodiorites and the lower one quartz diorite. Oceanic plateaus were modelled as three-layer structures for which the upper two layers are basalts and gabbros, as in normal ocean crust, and the lower layer is ultramafic peridotite. They included remanent magnetization in normal oceanic crust as described at the end of this section. Further details are in Hemant & Maus (2005) and Hemant (2003).

Remanent magnetization is significant in the oceans, the igneous nature of oceanic lithosphere resulting in the primary source being thermoremanent (TRM). It is acquired shortly after crustal formation at mid-ocean ridges (MORs) as magnetic grains cool through their blocking temperature and become 'frozen' in alignment with the ambient magnetic field (McElhinny & McFadden 2000). Subsequent low-temperature alteration of titanomagnetite to titanomaghemite leads to the exponential decay of TRM (Bleil & Petersen 1983) and complementary acquisition of secondary remanent magnetization components, notably chemical remanent magnetization (CRM).

Seafloor spreading anomalies show shape asymmetry relative to a square-wave anomaly pattern (skewness), resulting from deviations of the ambient field direction relative to the remanence and the strike of magnetic lineations; it can be corrected for by reducing anomalies to the geomagnetic pole. Anomalous skewness is the skewness that remains after this correction has been applied. Labrecque & Raymond (1985) and Raymond & Labrecque (1987) attempted to account for anomalous skewness by devising a model of crustal magnetization in which some TRM is lost and CRM is gained in the first 10 Myr. It explains many of the intermediate-wavelength satellite magnetic anomalies and short-wavelength sea-surface anomalies, including amplitude and skewness anomalies and enhanced

magnetization in the Cretaceous Quiet Zone (CQZ). They assumed a 500-m-thick magnetized layer corresponding to oceanic layer 2A, which comprises largely pillow basalts and lies directly beneath the sedimentary layer 1. Labrecque & Raymond (1985) assumed magnetization intensities varying from 8 to 15 A m^{-1} that decay exponentially away from the spreading axis. Raymond & Labrecque (1987) used a more complex model in which they allowed an original TRM at the ridge axis to decay exponentially with age while CRM is acquired, leaving a bulk magnetization intensity $A(t)$ as a function of crustal age:

$$A(t) = M_{\text{trm}}R(t)[1 + Pe^{-(t/\lambda)}]$$
$$+ (M_{\text{crm}}/\lambda) \sum_{t_a=0}^{T} R(t_a)e^{-[(t-t_a)/\lambda]}\Delta t_a, \qquad (1)$$

where t is a crustal age, P defines a partition between surviving and transient TRM [so it falls from $(1 + P)M_{\text{trm}}$ to M_{trm} over time], t_a is the time of CRM acquisition, M_{trm} is the total intensity of surviving TRM, $R(t)$ is a square wave with values ± 1 representing the polarity of the magnetic field as a function of time, the sum is over a sequence of intervals determined from plate reconstructions and λ is the decay time. The first term gives the decay of TRM and the second the growth of CRM. The decay time is of the order 5 Myr, so the time variation is complete within a few hundred kilometres of the ridge axis.

Dyment & Arkani-Hamed (1998) used this model to estimate remanence in the oceans and predict the magnetic field at satellite altitude, which they compared with their POGO- and MAGSAT-derived anomaly map (Arkani-Hamed *et al.* 1994). They concluded that remanence can explain not only the anomalies associated with crust generated during the Cretaceous Normal Superchron (CNS), but also several other weaker anomalies over the oceans, many of which are dominated by periods of a single polarity. The studies of both Raymond & Labrecque (1987) and Dyment & Arkani-Hamed (1998) needed to invoke magnetization estimates that are higher than those observed in laboratory studies of rock samples away from the spreading axis (Langel & Hinze 1998) in order to match the magnitude of the observed magnetic anomalies.

Hemant & Maus (2005) derived remanent VIM for the oceans only, following the methodology of Dyment & Arkani-Hamed (1998). They reproduced many observed magnetic anomalies, particularly over the continents, but much of the predicted oceanic signal was significantly underestimated and laterally offset relative to satellite observations. Unfortunately, they did not implement global plate circuits in their reconstruction of the ocean floor when estimating remanence; this may explain some of the lateral misfit between the satellite field and predictions from the magnetization model. The oceanic remanence model therefore needs to be recomputed.

In this paper, we compute lithospheric magnetization from first principles by a forward modelling approach using lithospheric properties such as crustal thickness, depth to Curie isotherm, stratigraphy, magnetic susceptibility and age-dependent magnetization intensity. We correct the plate reconstruction of Hemant & Maus (2005) and improve the oceanic remanence estimates. Finally, we combine our oceanic remanent magnetization model with the induced magnetization model of Hemant & Maus (2005) to produce a global model of VIM. The methods are described in Section 2, the results for the magnetization in Section 3, Section 4 gives a detailed comparison with observations and Section 5 gives the conclusions.

2 METHODS: ESTIMATION OF OCEANIC REMANENT MAGNETIZATION

We computed remanence in oceanic crust using eq. (1). The reversal time scale $R(t)$ was taken from Gradstein *et al.* (2005). After some experimentation, we chose $P = 5$ and $\lambda = 5$ Myr, the same as Raymond & Labrecque (1987), and retained their preferred ratio of CRM to TRM: $M_{crm}:M_{trm} = 4:1$. Raymond & Labrecque (1987) obtained the absolute value of the magnetization by setting $M_{trm} = 8.7$ A m^{-1} throughout a 500-m-thick layer at the ridge axis, presumably layer 2 A. This magnetization is unrealistically high but was needed to explain the magnitude of the magnetic anomalies; we use instead a more realistic value of 0.5 A m^{-1} distributed uniformly throughout the entire thickness of the oceanic lithosphere. The layer thickness is determined by the Curie isotherm depth for magnetite ($\sim$550 °C) using the GDH1 plate model of Stein & Stein (1992); it reaches almost 40 km in old oceanic lithosphere. This combination of magnetization and layer thickness gives the same VIM as Raymond & Labrecque (1987) after depth integration. The resulting remanence intensity–age profile is shown in Fig. 1. The largest features correspond to young ages (where young crust has strong TRM) and the CNS (where strong CRM develops during the long period of stable polarity). We integrate the remanence intensities over depth and time to give VIM at 1 Myr intervals.

We finally superimpose the resulting VIM–age profile onto a digital age grid of the ocean floor (Müller *et al.* 2008) to construct a map of oceanic remanent VIM amplitude estimates. We assume that TRM is acquired in a geocentric axial dipole field shortly after crust formation. The remanence intensity as a function of latitude is therefore multiplied by the usual dipole formula, $C = \sqrt{1 + 3\sin^2\theta}$, where θ is the colatitude of the MOR at the time of its formation.

The direction of remanence is determined by the orientation of the rock relative to the magnetizing field at the time of acquisition. TRM is aligned with the geomagnetic field direction that existed close to the palaeoposition of the ridge axis at the time of its formation. Low-temperature chemical alteration happens later and results in CRM with an orientation that may differ from the initial TRM direction due to seafloor spreading and ridge migration, but the difference is small because acquisition of CRM takes less than 10 Myr to complete. Furthermore, much of the rotation is about poles of rotation at high latitudes; since these poles broadly coincide with those of an axial dipole, the resulting change in the orientation of CRM is expected to be small. We therefore ignore this complication, which would in any case be difficult to implement accurately, and assume that CRM is aligned with TRM. The present-day direction of remanence is therefore determined from the original position of the MOR and the plate rotation sinceformation.

We calculate palaeo-MOR positions corresponding to present-day isochrons at 1 Myr intervals relative to a moving hotspot
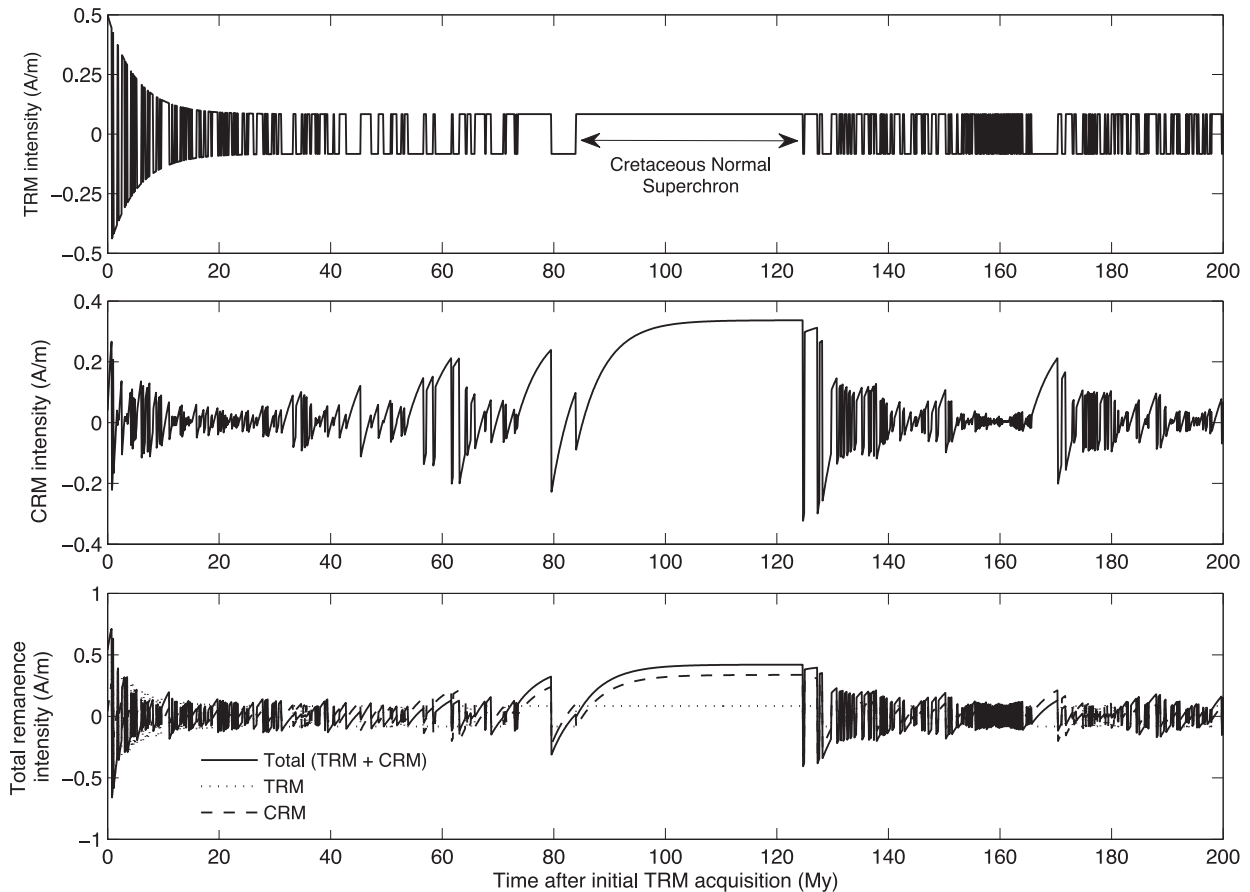

Figure 1. (a) Thermoremanent magnetization intensity is superimposed onto a geomagnetic polarity timescale (Gradstein *et al.* 2005) and allowed to decay exponentially with time constant $\lambda = 5$ Myr. (b) CRM is simultaneously acquired with the same time constant and a CRM:TRM ratio of 4:1. It is also superimposed onto the geomagnetic polarity timescale. (c) Total intensity as a function of age is the sum of TRM and CRM. See eq. (1) for the exact formula.
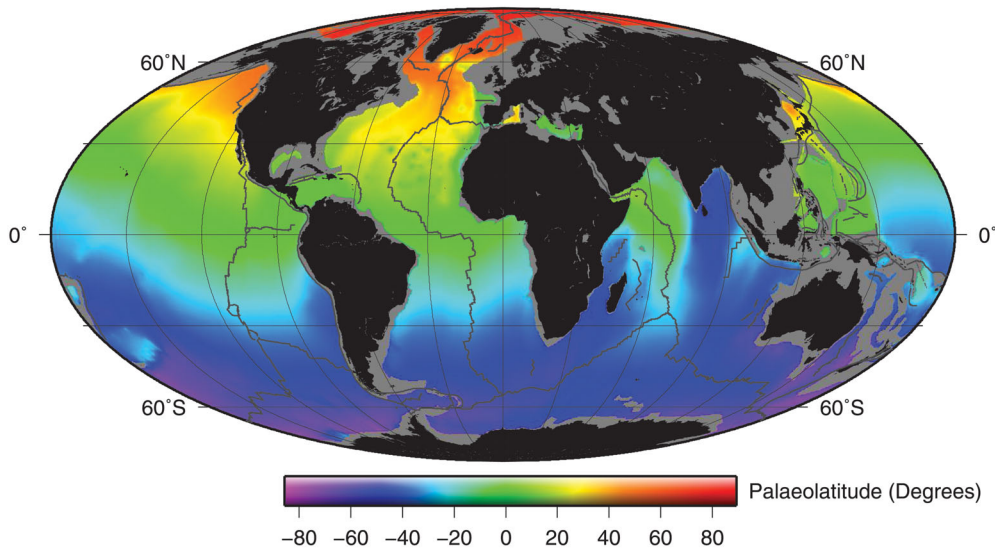
Figure 2. Latitudes at which present-day ocean floor was formed, interpolated onto a regular grid with cell size $0.25° \times 0.25°$. These were used to derive the amplitude of remanence, assuming that the paleofield was an axial dipole.

absolute mantle reference frame by implementing the plate reconstruction model of *Müller et al.* (2008). Our approach calculates the total finite rotation required to move each point in a densely populated global set of isochrons from their present-day to palaeo-MOR positions. This is an advance over previous work, which used the same finite rotation for entire plates for an extended time interval (Dyment & Arkani-Hamed 1998).

Fig. 2 shows the palaeolatitudes of reconstructed MORs. Palaeolatitudes are generally symmetrical about the present-day equator, suggesting that the present-day oceanic crust has not moved more than 20° or 30° north or south since it was formed. The most prominent exception to this trend is southeast of India where crust formed much further south, a result of the northwards drift of India after the break-up of Gondwana.

Multiplying the unit vectors of the direction of remanence by the VIM amplitudes gives the final $0.25° \times 0.25°$ vector remanent VIM model *RVIM-0*. This is added to the induced magnetization model of Hemant & Maus (2005) (henceforth referred to as *IVIM-0*) to give the global magnetization model *VIM-0*. The quarter-degree space grids *RVIM-0* and *IVIM-0* are expanded in the vector spherical harmonic set described in the companion paper (Gubbins *et al.* 2011):

$$\bar{M}(\theta, \phi) = \sum_{l,m} E_l^m Y_{l,l+1}^m(\theta, \phi) + I_l^m Y_{l,l-1}^m(\theta, \phi) + T_l^m Y_{l,l}^m(\theta, \phi)$$
$$= \mathcal{E} + \mathcal{I} + \mathcal{T}, \tag{2}$$

where $\bar{M}$ is the VIM (induced or remanent), $(Y_{l,l+1}^m, Y_{l,l-1}^m, Y_{l,l}^m)$ the vector harmonics and (E_l^m, I_l^m, T_l^m) are complex spherical harmonic coefficients. The series was truncated at $l = m = 256$ to provide an accurate representation on the quarter-degree spacing. Induced and remanent coefficients can be added to produce the total magnetization because of the linearity of eq. (2). The external potential field is described by the usual geomagnetic coefficients, which are simply related to the $\{I_l^m\}$:

$$g_l^m = \frac{\mu_0}{r_E} \sqrt{l\epsilon_m} \text{Re}(I_l^m), \tag{3}$$

$$h_l^m = -\frac{\mu_0}{r_E} \sqrt{l\epsilon_m} \text{Im}(I_l^m), \tag{4}$$

where

$$\epsilon_m = 2 - \delta_{m0}. \tag{5}$$

The other two sets of coefficients of the magnetization produce no external potential field. Further details are in the companion paper (Gubbins *et al.* 2011).

3 RESULTS FOR THE MAGNETIZATION

The full magnetization (induced and remanent) is shown in Fig. 3. Fig. 4 shows the spherical components of remanent VIM (M_r, M_θ, M_ϕ) for *RVIM-0*. Regions with strong radial components of VIM values correspond to lithosphere that is relatively thick and/or has stable geomagnetic polarity. Such regions are mainly constrained to CQZs ($\sim$84–125 Ma). VIM increases only slightly with age within these regions because remanence intensity reaches a plateau after the first 20 Myr of the CNS and magnetic crustal thickness based on GDH1 reaches its asymptotic value ($\sim$30–35 km) at around 100 Ma. Furthermore, no prominent VIM values exist close to MORs, where crust is thin. The M_ϕ component of VIM is significantly smaller than the other two; it results solely from the rotation of magnetized oceanic crust. Regions that have undergone significant rotation since the time of remanence acquisition exhibit relatively high values of M_ϕ.

The remanence is confined to the oceans except for oceanic plateaus and the induced magnetization is the vertically integrated susceptibility model of Hemant & Maus (2005) (Fig. 5). The global contribution of induced magnetization to the model *VIM-0* is much larger than that of remanence; this is primarily due to the absence of continental remanence in the model and the high continental magnetic crustal thicknesses in comparison to oceanic crust. Integration of the square of the induced and remanent contributions shows that their relative contributions to the energy of *VIM-0* are 95 and 5 per cent, respectively. The contribution of remanent magnetization over much of the oceans is small compared with induced magnetization because the occurrence of frequent geomagnetic reversals
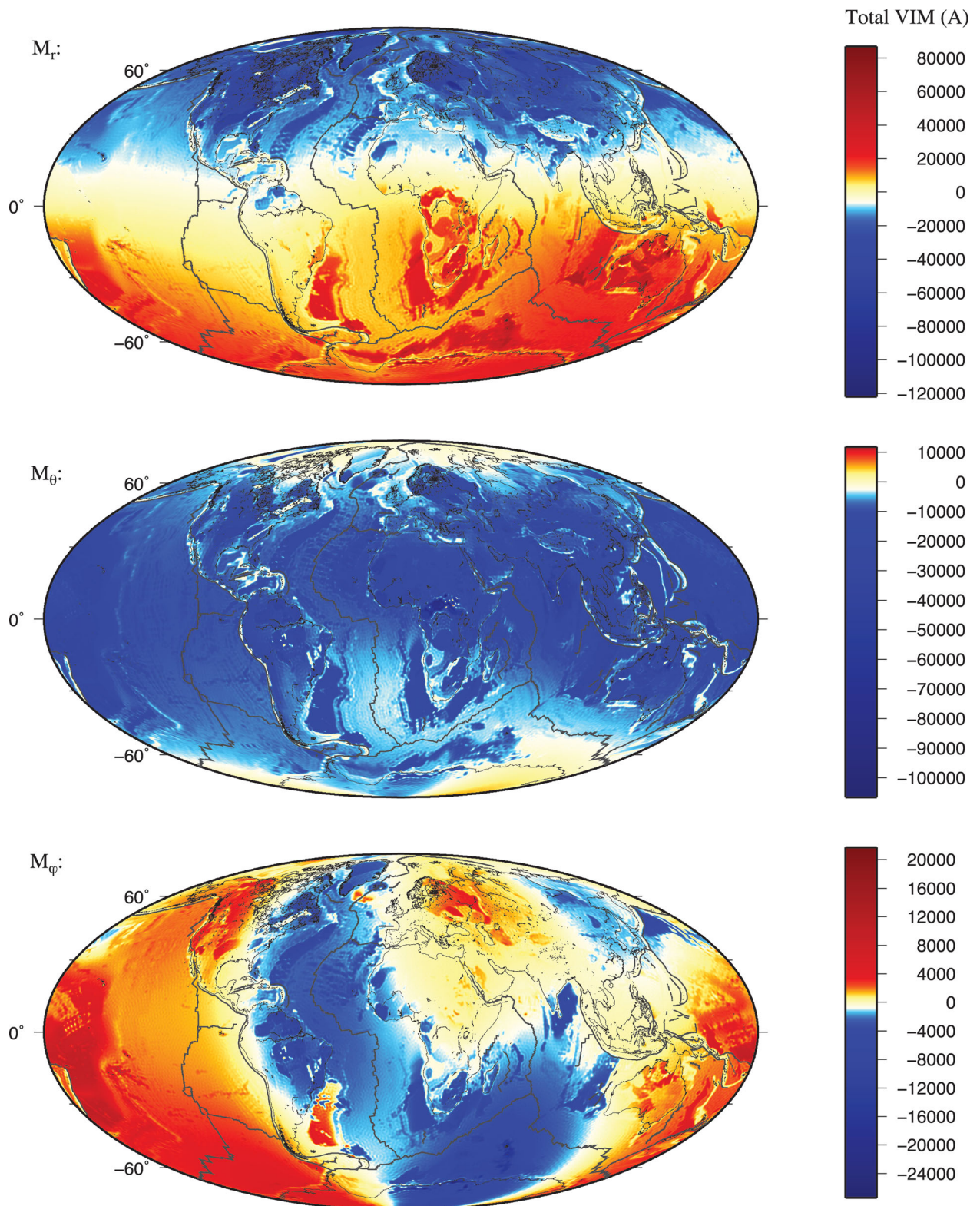
Figure 3. Global total (induced + remanent) VIM model, *VIM-0*, interpolated onto a regular 0.25° × 0.25° grid. M_r, M_θ and M_ϕ components are shown as top, centre and bottom figures, respectively. Colour scales differ for each component of magnetization.
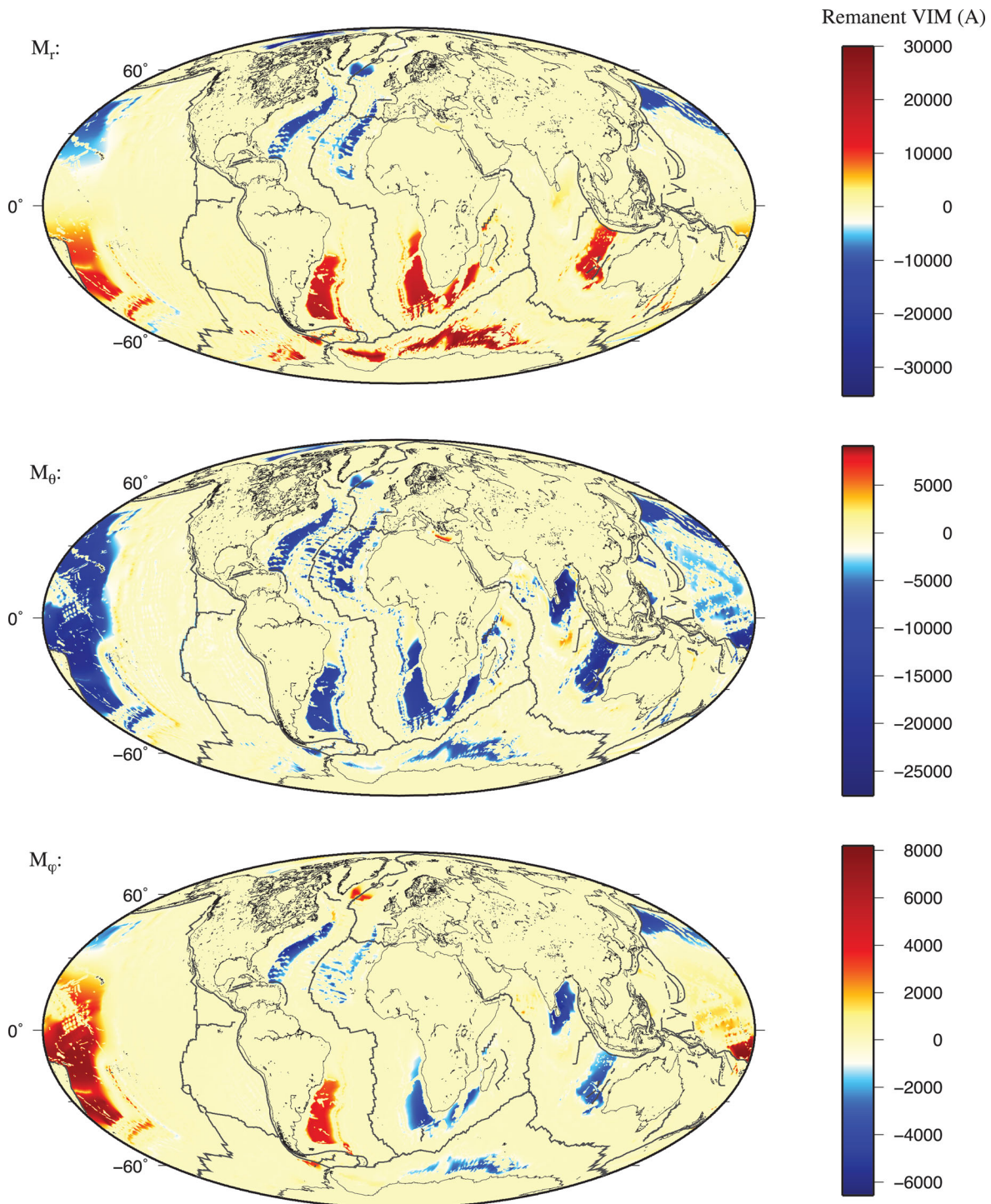
Figure 4. Global remanent VIM model *RVIM-0*, interpolated onto a regular $0.25° \times 0.25°$ grid. M_r, M_θ and M_ϕ components are shown as top, centre and bottom figures, respectively. The largest anomalies correspond to the CQZs. Here and in Figs 4, 5 and 6, tectonic plate boundaries are given by Müller *et al.* (2008). Note that colour scales are different for each component of magnetization.

does not allow significant CRM to accumulate over time. The total VIM distribution is predominantly dipolar, due to the strongly dipolar contribution of induced magnetization. The orientation of magnetization in CQZs is approximately parallel to the geomagnetic dipole in which the lithosphere was remanently magnetized.

This alignment is particularly strong in the Atlantic CQZs, where remanence has not undergone significant rotation since the time of acquisition. In contrast, the CQZ southeast of India exhibits a strong ϕ component of VIM arising from rotation following the break-up of Gondwana.
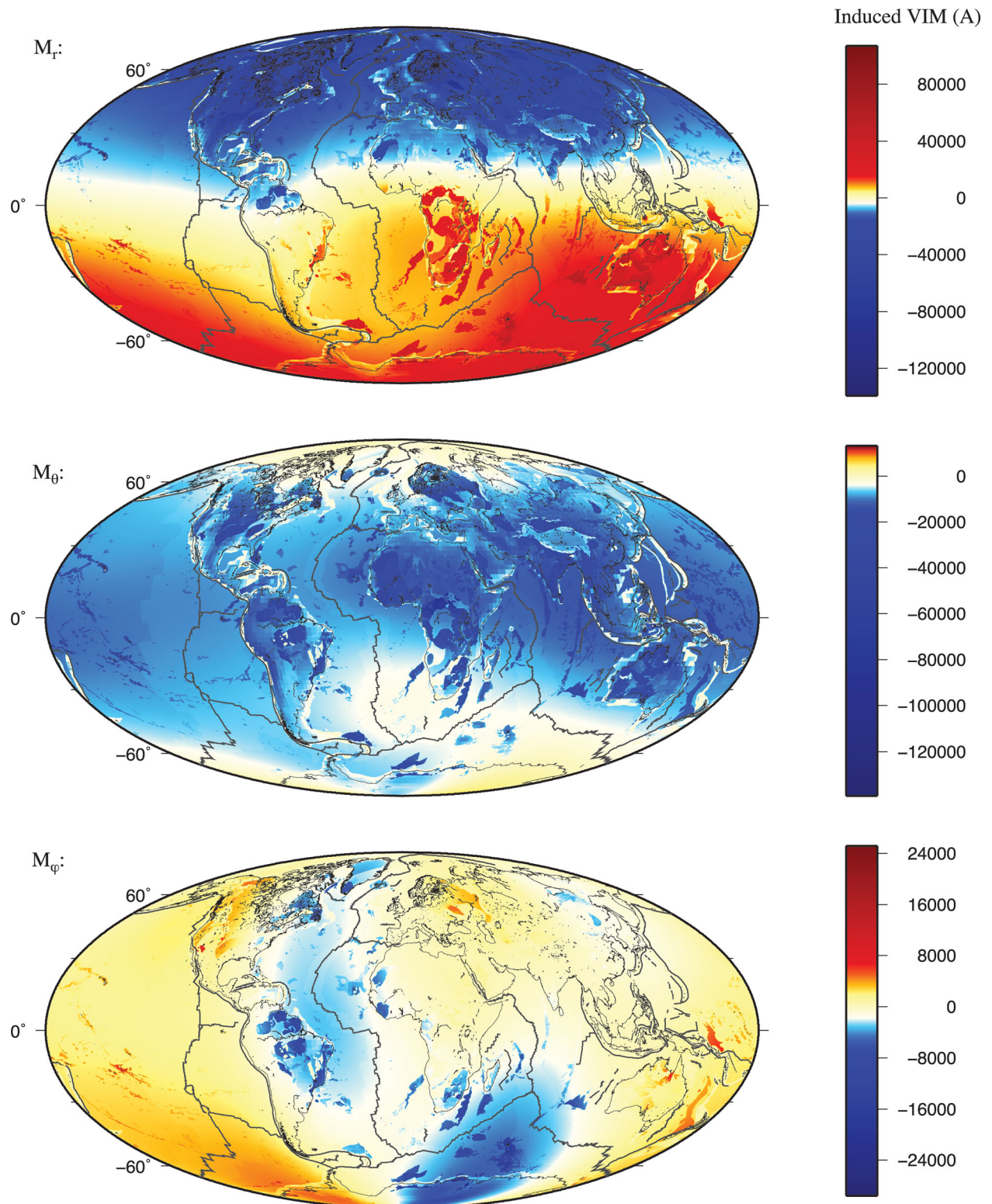
Figure 5. Global-induced VIM model, *IVIM-0*, interpolated onto a regular $0.25° \times 0.25°$ grid. M_r, M_θ and M_ϕ components are shown as top, centre and bottom figures, respectively. Colour scales differ for each component of magnetization. See Paper I (Gubbins *et al.* 2011) for further discussion of this magnetization.
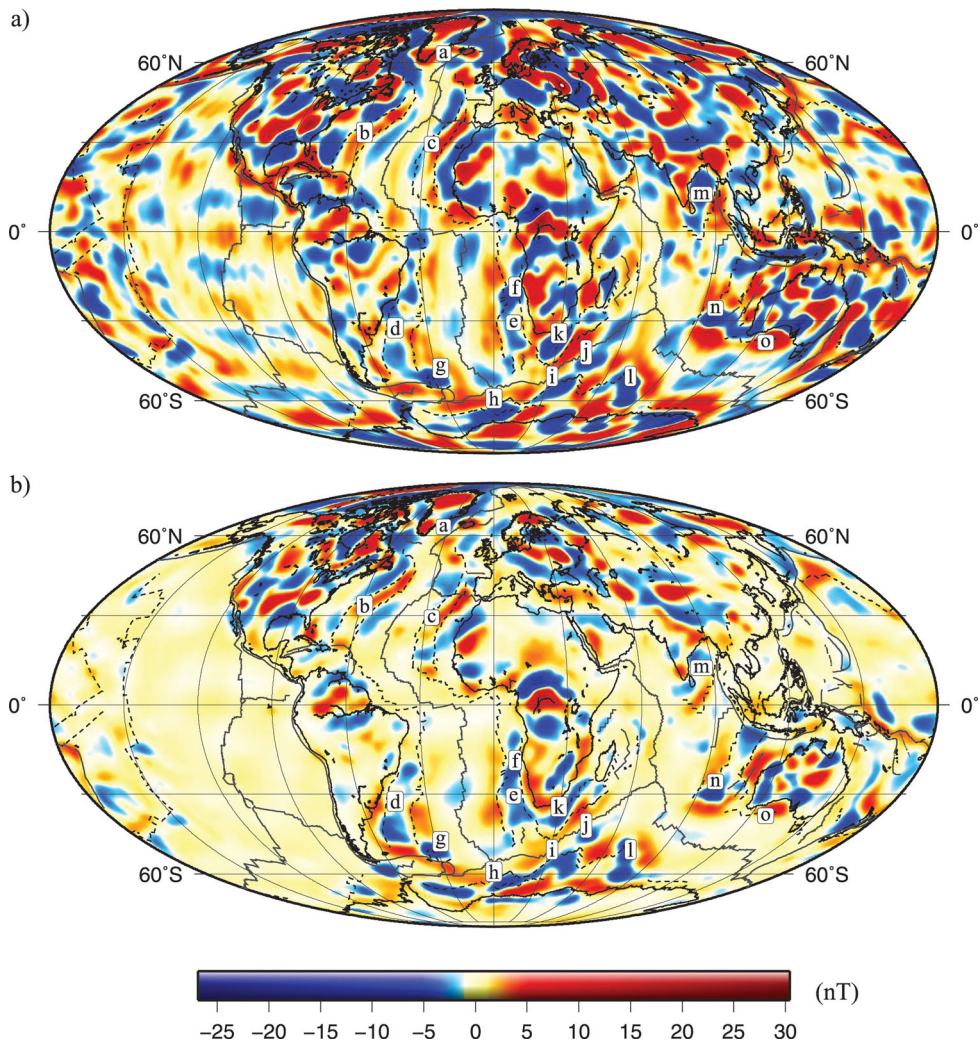
Figure 6. The vertical component of (a) MF7 potential magnetic field and (b) the potential magnetic field calculated from *VIM-0* (i.e. induced + remanent VIM) plotted at 350 km altitude, for spherical harmonic degrees 16–133. Map view is centred on the 0° meridian. Letters a–o correspond to regions referred to in the text and isochrons M0 and C34, which bound the CQZ are shown as heavy dashed lines.

4 COMPARISON WITH THE SATELLITE FIELD

We compare our predicted field with the satellite model MF7[1], an update of MF6 (Maus *et al.* 2008), both filtered to include only spherical harmonic degrees 16–133. Fig. 6(a) shows the vertical component of MF7 plotted at 350 km altitude for comparison with the *VIM-0*-predicted field in Fig. 6(b). There are many good correlations between prediction and observation over the continents and oceanic plateaux as described in Hemant & Maus (2005); here, we focus on anomalies over normal ocean floor. We acknowledge that MF7 is inherently subject to inaccuracies associated with data processing and collection that may lead to misfit between our predictions and MF7 (e.g. satellite orbital patterns, magnetometer malfunction, etc.). As it is difficult to separate such discrepancies from those associated with our predictions, the following discussion assumes that any misfit arises from problems with our magnetization estimates.

The CQZ crust produced during the CNS in the Atlantic and the Northeast Indian ocean is clearly seen in the predicted field: its magnetization may be attributed entirely to remanent magnetization. These zones are bounded by the present-day locations of magnetic anomalies M0 and C34, corresponding to 120.4 and 83.5 Ma isochrons, respectively. These isochrons are shown in Fig. 6 as heavy dashed lines; there is clearly a good correlation in both location and extent of the CQZ anomalies.

We compare the vertical components of MF7 and the predicted field at 15 specific locations labelled a–o in Figs 6(a) and 6(b) and 20 profiles that extend across oceanic regions and intersect significant anomalies (Fig. 7). The vertical component of the predicted field along these profiles has been separated into the individual contributions from our remanent, induced and total VIM estimates.

A strong positive anomaly is observed in MF7 that extends eastwards from Southern Greenland until the Faeroe-Rockall Plateau, east of Iceland (m). The corresponding anomaly in our predicted anomaly map is discontinuous as it is intersected by a negative anomaly that extends southwards along the east coast of Greenland.

[1] see[1]   http://www.geomag.us/models/MF7.html.   Last   accessed: 27/11/2012
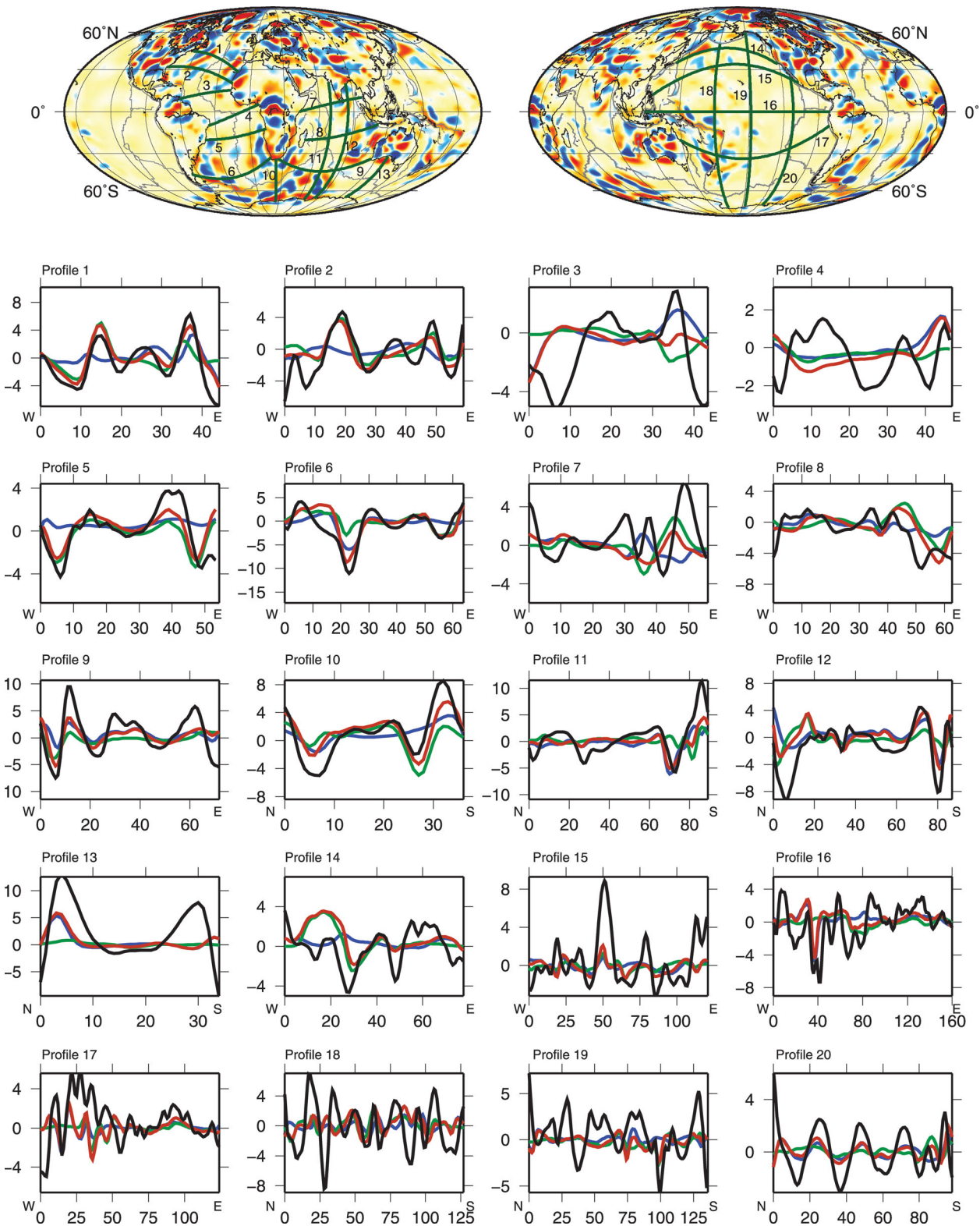
Figure 7. The vertical component (in nT) of MF7 (black) and the potential field calculated from induced VIM (*IVIM-0*, blue), remanent VIM (*RVIM-0*, green) and induced + remanent VIM (*VIM-0*, red), along profile lines 1–20. Plotted at 350 km altitude, for spherical harmonic degrees 16–133. Profile locations are shown on the top two maps of our predicted magnetic field (left: centred on the 20° meridian; right: centred on the 200° meridian).

Relatively strong anomalies associated with the CQZs are seen in both MF7 and the predicted magnetic field on both margins of the North and South Atlantic. In the North Atlantic, the region bounded by the M0 and C34 isochrons exhibits strong positive

anomalies that are flanked on either side by negative anomalies (b, c). On the North American side of the ridge, the lateral extent of the predicted positive and negative anomalies correlates well with the observations. On the African side of the ridge, much of the

observed western negative magnetic anomaly is either absent from the predicted magnetic field or of significantly lower amplitude. Fig. 6 shows that the positive CQZ anomaly is cross-cut by an elongated negative anomaly to the east. In contrast, MF7 shows this anomaly to broadly follow the coast of northwest Africa. Profile lines 1 and 2 in Fig. 7 cross-cut these anomalies and allow for evaluation of their amplitudes. The phases of the predicted CQZ anomalies correlate well with the MF7 observations on both sides of the North Atlantic. The negative anomalies are underpredicted by up to 1 nT. Profile 1 shows that the positive anomaly associated with the northwestern CQZ is ∼3 nT in MF7, but is overpredicted by ∼2 nT in our VIM model. Profile 2 is further south; the model successfully reproduces the amplitude of the positive anomaly as 4 nT. In both profiles 1 and 2, the positive and negative anomalies on the African side of the Mid-Atlantic Ridge are underpredicted. This may suggest that the contrast between the VIM within CQZs and adjacent oceanic crust needs to be increased to successfully reproduce them. Conversely, overpredicted anomalies may require reduction of the VIM contrast.

Negative magnetic anomalies associated with the CQZs in the South Atlantic are observed in both MF7 and our predicted field (d, e). The lateral extent of these anomalies is constrained by the M0 and C34 isochrons. A positive anomaly of the South American side of the ridge (d) cuts east–west into the CQZ in MF7 but is only seen to the east of this region in the predicted magnetic field. On the Eastern flank of the Mid-Atlantic Ridge, the negative anomaly in MF7 extends further north than the anomaly in the predicted field, which does not continue onto the African continent. This discrepancy may be partly attributed to the presence of the Walvis Ridge, which is characterized in MF7 by a negative anomaly off the West African coast (f). The induced VIM contribution to the predicted magnetic field may need to be extended northwards to improve its fit to MF7 in this region. This is supported by the eastern end of profile 5 in Fig. 7, where the negative anomaly in MF7 lies eastwards of that predicted by our model, and is in phase with a low that is associated with the induced part of the field. Profile 5 also shows that the CQZ anomalies on both sides of the ridge are underpredicted by 1–2 nT; the flanking positive anomaly to the west of the CQZ on the African side of the ridge (e) is underpredicted by ∼2 nT. A small contribution from induced VIM is shifted westwards relative to the main remanent contribution, producing two local maxima in the positive anomaly; this shape is clear in the MF7 anomaly, suggesting that the amplitudes of both the induced and remanent magnetization need to be increased in this region. Profile 6 shows a strong low of 10 nT in the MF7 magnetic field. Our predictions only slightly underpredict this anomaly, which comprises contributions from both remanent (associated with the CQZ) and induced VIM. The latter is attributed to the North Scotia Ridge (g).

MF7 shows a prominent negative anomaly in the Southwest Indian Ocean that lies over the Maud Rise (h). Our predictions partly reconstruct this anomaly, where the source of the magnetization is induced. The predicted anomaly extends eastwards, south of the C34 isochron and towards the Conrad Rise (i) and Crozet Plateau (j); MF7 anomalies over these three regions are, however, discrete. The location of the predicted negative anomalies in relation to the M0 and C34 isochrons may suggest that the remanent VIM contribution dominates over that of the induced contribution in our model, and should be adjusted accordingly.

The Agulhas Plateau lies off the southeast coast of Africa and is characterized by an elongated negative anomaly in MF7 (k) that ex-

tends northwards into Africa; the corresponding predicted anomaly is narrower and longer than in MF7 and does not extend into Africa: instead, it continues northeastwards towards the Mozambique Ridge. Comparison with the total VIM model suggests that much of the signal in this region may be attributed to high remanent VIM values associated with the CNS. The western end of Profile 9 in Fig. 7 shows that the amplitude in the central part of the predicted negative anomaly fits the observations reasonably well, and is dominated by the remanent part of the field. The northern end of Profile 10, however, shows that the predicted anomaly is significantly underestimated compared with the observations because either the induced part of the anomaly does not extend far enough to the south or the amplitude of the remanence is not sufficiently high. Misfit between predicted and observed anomalies in this region may be significantly improved by modifying the lateral extent of the VIM distribution.

A negative anomaly in the southern Indian Ocean (l) is associated with the Kerguelen–Gaussberg Ridge and is reconstructed reasonably well in the predicted field. The southern end of profile 11 shows that the amplitudes of the predicted and observed model are well matched at ∼5 nT; the predicted anomaly at this location could be shifted slightly southwards by extending the southern boundary of the Kerguelen–Gaussberg Ridge to improve the fit to the observations.

A strong negative anomaly is observed in MF7 in the Bay of Bengal region of the Northeast Indian Ocean (m); it is underpredicted by our model (northern end of Profile 12). According to the oceanic crustal age model of Müller *et al.* (2008), this region corresponds to a CQZ, but is also subject to significant age error. Detailed studies of isochron and fracture zone orientations and extents in this region (Desa *et al.* 2006) have revealed a complex tectonic history associated with the Early Cretaceous separation of India from Gondwana; relative plate motions during this time, the location of the continent-ocean boundary and the lateral extent of transitional crust remain somewhat ambiguous for the Bay of Bengal region (Desa *et al.* 2009). It is therefore unsurprising that our predicted model does not successfully reproduce the observed anomalies: it emphasizes the need for improved understanding of the tectonic history of the region.

The negative anomaly at (n) lies over the Broken Ridge, off the west coast of Australia. It extends eastwards over the Naturaliste Plateau and is flanked to the north and south by positive anomalies. While the anomaly over the Broken Ridge itself is reproduced in the predicted anomaly map, its eastward extension and much of the positive anomaly to the north are absent. Increasing the VIM contrast between the anomalous oceanic crust and the surrounding area and further consideration of the magnetic structure in the Naturaliste Plateau should improve the fit between the predictions and the observations.

A strong positive anomaly off the south coast of Australia is seen in both MF7 and the predicted magnetic anomaly map (o); the maximum amplitude of this anomaly along profile 13 is ∼12 nT and is significantly underpredicted by our model. This region forms part of the continental margin of South Australia, and may therefore be interpreted as an anomaly associated with induced magnetization at the continent-ocean boundary.

Many low-amplitude magnetic anomalies in the Pacific are present in the MF7 model but absent or underestimated in the predicted model (Fig. 6). Profiles 14–20 cross-cut the Pacific region and show that, while the amplitudes of many of the predicted anomalies are underestimated, their phases correlate. Profiles 18 and 20 are particularly good examples of this.

5 DISCUSSION AND CONCLUSIONS

Remanent magnetization of the oceanic lithosphere explains the majority of the signal recorded in the geomagnetic field at satellite altitude in the region of the CQZs and some other features in oceanic areas. This confirms the earlier conclusion of Dyment & Arkani-Hamed (1998).

Remanence is strong in the CQZs because the geomagnetic dipole stayed in the same polarity for a long time, allowing chemical remanence to build up to full strength. Induced magnetization is also strong in oceanic lithosphere, but uniformity of the ocean floor produces large-scale magnetization, which forms little potential magnetic field outside the Earth (Gubbins *et al.* 2011). The integral of the square of the VIM over the spherical surface gives an idea of the size of each contribution. Remanence contributes 24 per cent of this energy in the oceans, rather more to the part causing the observed geomagnetic field (the *I* part of Gubbins *et al.* 2011, eq. 2). The surface energy of the geomagnetic anomalies is measured by the Lowes energy $\sum(l+1)(g_l^{m2} + h_l^{m2})$, where the g_l^m, h_l^m are the geomagnetic coefficients and the sum is over all orders l and degrees m. The contribution of remanence to this is different from the contribution to the internal magnetization because of the factors involving l and m between the relevant spherical harmonic coefficients (Gubbins *et al.* 2011, eqs 32–33). Remanence contributes 39 per cent to the geomagnetic Lowes energy, greater than you would expect from a simple comparison of its strength compared to the induced magnetization. Remanence is generally very weak at these wavelengths because of the rapidity of polarity reversals, it dominates geomagnetic anomalies in places where reversals were infrequent at the time of formation of the lithosphere because the induced component produces rather little magnetic field outside the Earth.

The remanent magnetization and susceptibilities used in our model tend to be rather high compared to what would be dictated strictly by laboratory measurements (Langel & Hinze 1998). Despite this, the lithospheric magnetic field is still stronger than the predicted field in many, but by no means all, areas. This is surprising because an idealized model might be expected to produce a larger signal in the wavelengths of interest, whereas in the Earth, one might expect the structures to be broken up, particularly on continents. More significantly, all studies use VIM, a simple integral in depth, whereas the correct formula for the magnetic field involves moments of the magnetization (Gubbins *et al.* 2011, eq. 8) with a factor $[(r_E - d)/r_E]^l$, where r_E is the Earth's radius, d is the depth, and l is the spherical harmonic degree. This factor is close to 1 for low degrees because the magnetized layer is thin compared to Earth's radius. It is, however, always less than one and becomes significantly so at high degree, to 2/3 by degree 50, for example. The deeper magnetizations are de-emphasized the most.

The model fails to predict much structure in the oceans away from the CQZs: note the almost complete absence of anomalies in the eastern Pacific in Fig. 6b. This is again not surprising because the ocean floor is very uniform, the Curie depth relatively shallow, and reversals were frequent during crust formation, causing the remanence on the length scales associated with satellite altitude (i.e. 350 km) to be averaged out: for example, a spreading rate of 6 cm yr^{-1} and reversal frequency of 3 per million years gives a stripe width of only 20 km, whereas a typical wavelength at a high spherical harmonic degree in a satellite model ($l = 100$) is of order 200 km.

Satellite model MF7 (Fig. 6a) is not unusual in showing substantial anomalies throughout the eastern Pacific and in other parts of the oceans away from ridges and CQZs. This signal remains to be explained. Four possibilities come to mind:

(i) The oceanic crust is fractured and altered more than we assume. This possibility could be explored in detailed local studies. Estimates of crustal magnetization are almost entirely based on near-surface samples, so it is at the surface that our estimates should be the most reliable. The geomagnetic signal must therefore arise from departures from uniformity in oceanic lithosphere.

(ii) The upper mantle is more highly magnetized than we expect, and is relatively non-uniform. Magnetization of the deeper lithosphere is not at all well known. There is some recent evidence that titanomagnetite increases its magnetization properties under pressure and retains that stronger magnetization after the pressure is removed (Gilder & Goff 2008). The upper mantle could therefore be more magnetic than has been supposed so far: if so, the anomalies seen at satellite altitude could reflect upper mantle structure and dynamics.

(iii) Oceanic lithosphere could be locally underplated by magnetized continental lithosphere or by serpentinized exhumed mantle (Sibuet *et al.* 2007). Hoernle *et al.* (2011) provide supportive evidence for the former, with the suggestion of shallow recycling of continental lithosphere beneath the Indian Ocean. If such a link between underplating and the magnetic anomalies could be established, the satellite models could provide clues to lithospheric structure and past history.

(iv) Finally, some signal may come from the core field. Core field dominates at long wavelength and is swamped by the crustal field above spherical harmonic degrees 16, but there will still be places where the crustal field is weak or the small-scale core field exceptionally strong. The spectrum of the core field is approximately flat at the core–mantle boundary out to degree 14 or so; beyond that it could remain flat or even rise. The upward continuation factor from the core greatly reduces the higher harmonics, but they could contribute to features such as those in the east Pacific at the 1–5 nT level. Improving our knowledge of the lithospheric component would allow us to remove its contribution from the total field and identify the extent of these core field contributions; this would therefore greatly advance our understanding of core processes.

ACKNOWLEDGMENTS

REFERENCES

Arkani-Hamed, J., Langel, R.A. & Purucker, M., 1994. Scalar magnetic anomaly maps of earth derived from POGO and Magsat data, *J. geophys. Res.,* **99,** 24 075–24 090.

Bassin, C., Laske, G. & Masters, G., 2000. The current limits of resolution for surface wave tomography in North America, *EOS, Trans. Am. geophys. Un.,* **81**(48), Fall Meet. Suppl., Abstract S12A-03.

Bleil, U. & Petersen, N., 1983. Variations in magnetization intensity and low-temperature oxidation of ocean floor basalts, *Nature,* **301,** 384–388.

Desa, M., Ramana, M. & Ramprasad, T., 2006. Seafloor spreading magnetic anomalies south off Sri Lanka, *Mar. Geol.,* **229,** 227–240.

Desa, M., Ramana, M. & Ramprasad, T., 2009. Evolution of the late cretaceous crust in the equatorial region of the northern Indian ocean and its implication in understanding the plate kinematics, *Geophys. J. Int.,* **177**(3), 1265–1278.

Dyment, J. & Arkani-Hamed, J., 1998. Contribution of lithospheric remanent magnetization to satellite magnetic anomalies over the world's oceans, *J. geophys. Res.,* **103,** 15 423–15 441.

Friis-Christensen, E. & Luhr, H., 2006. Swarm: a constellation to study the Earth's magnetic field, *Earth Planets Space,* **58,** 351–358.

Friis-Christensen, E., Luhr, H., Hulot, G., Haagmans,, R. & Purucker, M., 2009, Geomagnetic research from space, *EOS, Trans. Am. geophys. Un.,* **90**(23), 213–214.

Gilder, S.A. & Goff, M.L., 2008. Systematic pressure enhancement of titanomagnetite magnetization, *Geophys. Res.Lett.,* **35**(10), L10302, doi:10.1029/2008GL033325.

Gradstein, F.M., Ogg, J.G. & Smith, A.G., 2005. *A Geologic Timescale 2004,* Cambridge University Press.

Gubbins, D., Ivers, D., Masterton, S.M. & Winch, D.E., 2011. Analysis of lithospheric magnetisation in vector spherical harmonics, *Geophys. J. Int.,* **187,** 99–117.

Hemant, K., 2003. Modelling and interpretation of global lithospheric magnetic anomalies, *PhD thesis,* Freie University, Berlin.

Hemant, K. & Maus, S., 2005. Geological modeling of the new CHAMP magnetic anomaly maps using a geographical information system technique, *J. geophys. Res.,* **110**(B12103), doi:10.1029/2005JB003837.

Hoernle, K., Hauff, F., Werner, R., van den Bogaard, P., Gibbons, A.D., Conrad, S. & Muller, R.D., 2011. Origin of Indian Ocean seamount province by shallow recycling of continental lithosphere, *Nature Geosci.,* **4**(12), 883–887.

Labrecque, J.L. & Raymond, C.A., 1985. Seafloor spreading anomalies in the Magsat field of the North Atlantic, *J. geophys. Res.,* **90,** 2565–2575.

Langel, R.A. & Hinze, W.J., 1998. *The Magnetic Field of the Earth's Lithosphere—The Satellite Perspective,* pp. 269–270, Cambridge University Press.

Maus, S. & Haak, V., 2003. Magnetic field annihilators: invisible magnetization at the magnetic equator, *Geophys. J. Int.,* **155,** 509–513.

Maus, S. *et al.*, 2008. Resolution of direction of oceanic magnetic lineations by the sixth-generation lithospheric magnetic field model from champ satellite magnetic measurements, *Geochem. Geophys. Geosyst.,* **9,** Q07021, doi:10.1029/2008GC001949.

Maus, S. *et al.*, 2009. EMAG2: A 2-arc min resolution Earth Magnetic Anomaly Grid compiled from satellite, airborne, and marine magnetic measurements, *Geochem.Geophys. Geosyst.,* **10**(8), Q08005, doi:10.1029/2009GC002471.

McElhinny, M.W. & McFadden, P.L., 2000. *Paleomagnetism: Continents and Oceans,* Academic Press, San Diego.

Müller, R.D., Sdrolias, M., Gaina, C. & Roest, W.R., 2008. Age, spreading rates, and spreading asymmetry of the world's ocean crust, *Geochem. Geophys. Geosyst.,* **9,** doi:10.1029/2007GC001743.

Nataf, H.C. & Ricard, Y., 1996. 3SMAC: an a priori tomographic model of the upper mantle based on geophysical modeling, *Phys. Earth planet. Inter.,* **95,** 101–122.

Olsen, N. & Kotsiaros, S., 2011. Magnetic satellite missions and data, in *Geomagnetic Observations and Models,* eds Mandea, M. & Korte, M., vol. 5 of IAGA Special Sopron Book Series, pp. 27–44, Springer, Netherlands.

Raymond, C.A. & Labrecque, J.L., 1987. Magnetization of the oceanic crust - thermoremanent magnetization of chemical remanent magnetization?, *J. geophys. Res.,* **92,** 8077–8088.

Sibuet, J., Srivastava, S. & Manatschal, G., 2007. Exhumed mantle-forming transitional crust in the Newfoundland-Iberia rift and associated magnetic anomalies, *J. geophys.Res.,* **112**(B6), B06105, doi:10.1029/2005JB003856.

Stein, C. & Stein, S., 1992. A model for the global variation in oceanic depth and heat flow with lithospheric age, *Nature,* **359,** 123–129.

Taylor, S.R. & McLennan, S.M., 1985. *The Continental Crust: Its Composition and Evolution,* p. 312, Blackwell Scientific Publications.

Wasilewski, P.J. & Mayhew, M.A., 1992. The Moho as a magnetic boundary revisited, *Geophys. Res. Lett.,* **19,** 2259–2262.